photonics

MDPI

Article

Microwave Photonic Frequency Multiplier with Low Phase Noise Based on an Optoelectronic Oscillator

Hao Luo, Jinlong Yu, Ju Wang, Chuang Ma, Xu Han, Xuemin Su, Ye Gao and Shi Jia *

School of Electrical and Information Engineering, Tianjin University, Tianjin 300072, China; hello_hluo2020@tju.edu.cn (H.L.); yujinlong@tju.edu.cn (J.Y.); wangju@tju.edu.cn (J.W.); machuang@tju.edu.cn (C.M.); hanxu1016@tju.edu.cn (X.H.); xueminsu@tju.edu.cn (X.S.); gaoye0610@tju.edu.cn (Y.G.)

* Correspondence: tjujession@tju.edu.cn

Abstract: A microwave photonic frequency multiplier with low phase noise based on an optoelectronic oscillator (OEO) is proposed and experimentally demonstrated. In this scheme, a dual-parallel Mach–Zehnder modulator (DPMZM) is employed to generate the third-harmonic frequency of the input radio frequency (RF) signal, while the oscillation frequency of the OEO is also three times the RF signal frequency. By adjusting the bias voltages of different arms in the DPMZM, a triple-frequency signal with a high side-mode suppression ratio of 64.8 dB can be obtained. The experimental results indicate that the output of the frequency-multiplier has a better single-sideband phase noise value, for instance, −126 dBc/Hz@10 kHz at 20.019 GHz. It has improvements of 34 dB and 43.5 dB compared with the input RF signal and the simulated electrical frequency tripler module, respectively.

Keywords: microwave photonics; optoelectronic oscillator; frequency multiplier; dual-parallel Mach–Zehnder modulator

1. Introduction

Microwave photonic technology has attracted increasing interest due to its wide applications in optical wireless communication [1], radar [2], aerospace [3] and so on [4]. In most of these applications, microwave signal generation via photonic frequency multiplication [5,6] plays a key role. Therefore, this topic has drawn a great deal of research attention.

Traditionally, microwave signals with frequency multiplication are generated by purely electronic methods, but the frequencies are limited by the bandwidth of the electronic devices. The involved electrical components increase the cost of the system, especially for high-frequency microwave signal generation. Moreover, a phase noise deterioration of $20\log_{10}(N)$ occurs during the frequency multiplication process, where N is the multiplication factor [7]. In comparison, photonic generation of frequency-multiplying microwave signals has great advantages due to its features, e.g., reconfigurability, a high bandwidth capability, low phase noise deterioration, and immunity to electromagnetic interference [8].

Thus far, various photonic approaches for frequency multiplication have been proposed and demonstrated [9,10], such as optical heterodyne techniques [11,12], external modulation [13–15], the use of optical nonlinear effects of stimulated Brillouin scattering (SBS) [16,17], and so on. In [18], low-noise repetition-rate multiplication is obtained via harmonic injection locking and gain-saturated amplification. However, the side-mode suppression ratio (SMSR) is only 33 dB, as determined by the injection power. Kim et al. [19] proposed a tunable repetition-rate multiplication method based on harmonic injection locking of mode-locked lasers. In the system, the resulting maximum SMSR is 41 dB for multiplication by a factor of two. Moreover, phase noise deterioration occurs for high repetition-rate multiplication. In [20–22], external modulation with frequency multiplication is widely exploited. Except for different modulation indexes and phase shifters

check for updates

Citation: Luo, H.; Yu, J.; Wang, J.; Ma, C.; Han, X.; Su, X.; Gao, Y.; Jia, S. Microwave Photonic Frequency Multiplier with Low Phase Noise Based on an Optoelectronic Oscillator. *Photonics* **2024**, *11*, 588. https://doi.org/10.3390/photonics11070588

Received: 27 May 2024
Revised: 17 June 2024
Accepted: 21 June 2024
Published: 24 June 2024

between radio frequency (RF) driving signals, these schemes all use cascaded or dual-parallel Mach–Zehnder modulators (MZMs) to implement frequency multiplication of the RF driving signal. However, the SMSRs of these methods are low, and the phase noise of the optical microwave signal is affected by the driving signal. In realizing frequency multiplication, the use of SBS can also be promising because of the narrow frequency spacing. In [23], the sextuple Stokes signal (60 GHz: 0.48 nm) are successfully demonstrated utilizing a triple unidirectional ring laser cavity. Bai et al. [24] propose the generation of a 21.66-GHz microwave signal based on cascaded stimulated Brillouin scattering effects. Although these methods can generate frequency-multiplying microwave signals, the main limitation of SBS is that the generated microwave signals are restricted to the Brillouin frequency (f_B, ~11 GHz) [25].

On the other hand, optoelectronic oscillators (OEOs) can be configured as self-starting microwave signal generators [26,27]. An OEO shows prominent performance in terms of high spectral purity and ultralow phase noise [28,29], which enables high-quality frequency multiplication signal generation. In [30], a 4.03 GHz fundamental oscillation signal and its frequency-sextupled microwave signal at 24.18 GHz are generated by a dual-loop OEO. The 24.18 GHz microwave signal is 18.5 dB greater than the other harmonics. The measured single-sideband (SSB) phase noise at a 100 kHz offset frequency is approximately −98.6 dBc/Hz. Wu et al. [31] propose a tunable frequency-doubling OEO based on a single-bandpass microwave photonic filter consisting of an MZM. In the experiment, a 13.7 GHz frequency-doubling microwave signal is generated. However, this scheme requires careful adjustment of the polarizer angle between the polarizing beam splitter and the combiner. Moreover, the SMSR of the frequency-doubling signal is only approximately 44 dB. Compared with all the schemes mentioned above, if the low phase noise and high spectral purity of an OEO are fully utilized, then a microwave photonic frequency-multiplier system can be obtained. For practicability, a simpler high-SMSR and low-phase-noise frequency-multiplier OEO is expected.

In this letter, we propose and experimentally demonstrate a photonic frequency-tripled signal generator based on an OEO, in collaboration with a DPMZM. The sub-MZMs in the DPMZM are independently modulated by the input RF signal and the oscillated triple-frequency signal from the OEO. Under the appropriate bias voltages of the DPMZM, a frequency-tripled signal of the input RF signal frequency can be generated. In the stable state, the OEO works in the injection-locked state with triple-frequency oscillation, which has low phase noise without phase noise deterioration. A proof-of-concept experiment is carried out to verify the feasibility of the proposed scheme. In the experiment, a 20.019-GHz tripled signal with an SMSR as high as 64.8 dB is successfully obtained. The measured SSB phase noise is −126 dBc/Hz at a 10-kHz offset from the carrier, which is a substantial improvement of 34 dB and 43.5 dB from the input RF signal and simulated electric triple frequency module, respectively.

2. Principle

The DPMZM is more than crucial in the proposed system and acts not only as an electro-optical modulation device for the OEO but also as a frequency multiplication device for the input RF signal. The DPMZM contains two MZMs, denoted as MZM1 and MZM2, respectively. The two MZMs are nested within a third parent, MZM3, as shown in Figure 1. Three independent bias voltages (V_{bias1}, V_{bias2}, V_{bias3}) are used to control the modulation mode and two radio frequency inputs.

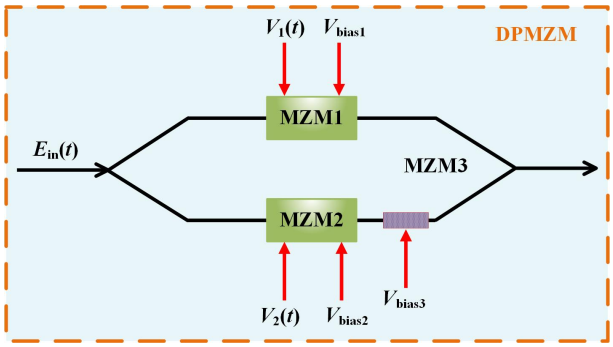

Figure 1. Internal structure of the DPMZM.

Assume that continuous wave (CW) light from a laser diode (LD) is sent to the DPMZM, the output optical fields of MZM1 and MZM2 can be given as [32]:

$$\begin{cases} E_{MZM1}(t) = \frac{E_{in}(t)}{\sqrt{2}} \cos\left[\varphi_1 + \frac{\pi V_1(t)}{V_\pi}\right] \\ E_{MZM2}(t) = \frac{E_{in}(t)}{\sqrt{2}} \cos\left[\varphi_2 + \frac{\pi V_2(t)}{V_\pi}\right] \end{cases} \tag{1}$$

where $E_{in}(t)$ denotes the amplitude of the optical field and $\varphi_1 = \pi V_{\text{bias1}}/V_\pi$ and $\varphi_2 = \pi V_{\text{bias2}}/V_\pi$ are the phase shifts determined by bias voltages V_{bias1} and V_{bias2}, respectively. V_π is the half-wave voltage of the modulator. $V_1(t)$ and $V_2(t)$ represent the input RF modulation signals of MZM1 and MZM2. Let $V_1(t) = V_{m1}\cos(\omega_{m1}t)$ and $V_2(t) = V_{m2}\cos(\omega_{m2}t)$, where V_m and ω_m are the amplitude and angular frequency of the RF signal, respectively. The modulation indices of MZM1 and MZM2 are defined as $\beta_1 = \pi V_{m1}/V_\pi$ and $\beta_2 = \pi V_{m2}/V_\pi$. Then, (1) can be rewritten as:

$$\begin{cases} E_{\text{MZM1}}(t) = \frac{E_{in}(t)}{\sqrt{2}} \cos\varphi_1 \cos\left[\beta_1 \cos(\omega_{m1}t)\right] \\ \qquad\qquad - \frac{E_{in}(t)}{\sqrt{2}} \sin\varphi_1 \sin\left[\beta_1 \cos(\omega_{m1}t)\right] \\ E_{\text{MZM2}}(t) = \frac{E_{in}(t)}{\sqrt{2}} \cos\varphi_2 \cos\left[\beta_2 \cos(\omega_{m2}t)\right] \\ \qquad\qquad - \frac{E_{in}(t)}{\sqrt{2}} \sin\varphi_2 \sin\left[\beta_2 \cos(\omega_{m2}t)\right] \end{cases} \tag{2}$$

Applying the Jacobi–Anger expansion to (2), we have:

$$\begin{cases} E_{\text{MZM}}(t) = \frac{E_{\text{in}}(t)\cos\varphi_1}{\sqrt{2}}[J_0(\beta_1) + 2\sum_{k=1}^{+\infty}(-1)^k J_{2k}(\beta_1) \\ \cos(2k\omega_{m1}t)]) - \frac{E_{\text{in}}(t)\sin\varphi_1}{\sqrt{2}}[2\sum_{k=0}^{+\infty}(-1)^k J_{2k+1}(\beta_1) \\ \cos(2k+1)\omega_{m1}t] \\ E_{\text{MZM}}(t) = \frac{E_{\text{in}}(t)\cos\varphi_2}{\sqrt{2}}[J_0(\beta_2) + 2\sum_{k=1}^{+\infty}(-1)^k J_{2k}(\beta_2) \\ \cos(2k\omega_{m2}t)]) - \frac{E_{\text{in}}(t)\sin\varphi_2}{\sqrt{2}}[2\sum_{k=0}^{+\infty}(-1)^k J_{2k+1}(\beta_2) \\ \cos(2k+1)\omega_{m2}t] \end{cases} \tag{3}$$

where $J_n(\beta)$ is the Bessel function of the first kind of order n. The modulation process can generate multiple spectral lines with frequency intervals of ω_m. The amplitude distribution of these spectral lines is determined by the variation in the β-parameterized Bessel function. Therefore, based on the properties of Bessel functions, the higher-order harmonic compo-

nents have no obvious influence on the output signals of the MZM [33]. Consequently, the modulated optical signal can be approximately represented as:

$$\begin{cases} E_{MZM1}(t) = \frac{E_{in}(t)}{\sqrt{2}} \cos\varphi_1 \left[J_0(\beta_1) - 2J_2(\beta_1)\cos(2\omega_{m1}t)\right] \\ -\frac{E_{in}(t)}{\sqrt{2}} \sin\varphi_1 [2J_1(\beta_1)\cos(\omega_{m1}t) - 2J_3(\beta_1)\cos(3\omega_{m1}t)] \\ E_{MZM2}(t) = \frac{E_{in}(t)}{\sqrt{2}} \cos\varphi_2 [J_0(\beta_2) - 2J_2(\beta_2)\cos(2\omega_{m2}t)] \\ -\frac{E_{in}(t)}{\sqrt{2}} \sin\varphi_2 [2J_1(\beta_2)\cos(\omega_{m2}t) - 2J_3(\beta_2)\cos(3\omega_{m2}t)] \end{cases} \tag{4}$$

In our proposed frequency multiplication system, the electrical feedback signal (ω_{m2}) of the OEO serves as the driving signal to MZM2 and satisfies the condition $\omega_{m2} = 3\omega_{m1}$. In this case, ignoring harmonic components above the 3-order, (4) can be written as follows:

$$\begin{cases} E_{MZM1}(t) = \frac{E_{in}(t)}{\sqrt{2}} \cos\varphi_1 \left[J_0(\beta_1) - 2J_2(\beta_1)\cos(2\omega_{m1}t)\right] \\ -\frac{E_{in}(t)}{\sqrt{2}} \sin\varphi_1 \left[2J_1(\beta_1)\cos(\omega_{m1}t) - 2J_3(\beta_1)\cos(3\omega_{m1}t)\right] \\ E_{MZM2}(t) = \frac{E_{in}(t)}{\sqrt{2}} \cos\varphi_2 J_0(\beta_2) - \frac{2E_{in}(t)}{\sqrt{2}} \sin\varphi_2 J_1(\beta_2) \\ \times \cos(3\omega_{m1}t) \end{cases} \tag{5}$$

Considering that the role of V_{bias3} is to change the phase difference between MZM1 and MZM2, $\varphi_3 = \pi V_{\text{bias3}}/V_\pi$ is defined as the phase shift introduced by V_{bias3}. Therefore, the optical signal at the output of the DPMZM can be expressed as:

$$\begin{aligned} E_{DPMZM}(t) = {} & \frac{E_{in}(t)}{\sqrt{2}} \cos\varphi_1 \left[J_0(\beta_1) - 2J_2(\beta_1)\cos(2\omega_{m1}t)\right] \\ & - \sqrt{2}E_{in}(t) \sin\varphi_1 [J_1(\beta_1)\cos(\omega_{m1}t) - J_3(\beta_1)\cos(3\omega_{m1}t)] \\ & + \frac{E_{in}(t)}{\sqrt{2}} \cos(\varphi_2 + \varphi_3) J_0(\beta_2) \\ & - \sqrt{2}E_{in}(t) \sin(\varphi_2 + \varphi_3) J_1(\beta_2) \cos(3\omega_{m1}t) \end{aligned} \tag{6}$$

Consequently, if this signal is detected by a photodetector (PD), then the photocurrent can be obtained as follows:

$$\begin{aligned} I_{out(3\omega_{m1})} & \propto E_{DPMZM}(t) \cdot E^*_{DPMZM}(t) \\ & \propto DC + 2E^2_{in}(t)[A\cos(\omega_{m1}t) \\ & + B\cos(2\omega_{m1}t) + C\cos(3\omega_{m1}t)] \end{aligned} \tag{7}$$

where the coefficients for different frequency components are given by:

$$\begin{cases} A = \cos\varphi_1 \sin\varphi_1[J_2(\beta_1)J_1(\beta_1) \\ \quad -J_0(\beta_1)J_1(\beta_1) - J_2(\beta_1)J_3(\beta_1)] \\ \quad +\cos\varphi_1 \sin(\varphi_2+\varphi_3)J_1(\beta_2)J_2(\beta_1) \\ \quad -\sin\varphi_1 \cos(\varphi_2+\varphi_3)J_0(\beta_2)J_1(\beta_1) \\ \\ B = \sin^2\varphi_1\left[\frac{1}{2}J_1^2(\beta_1) - J_1(\beta_1)J_3(\beta_1)\right] \\ \quad +\sin\varphi_1 \sin(\varphi_2+\varphi_3)J_1(\beta_2)J_1(\beta_1) \\ \quad -\cos^2\varphi_1 J_0(\beta_1)J_2(\beta_1) \\ \quad -\cos\varphi_1 \cos(\varphi_2+\varphi_3)J_0(\beta_2)J_2(\beta_1) \\ \\ C = \cos\varphi_1 \sin\varphi_1[J_0(\beta_1)J_3(\beta_1) + J_2(\beta_1)J_1(\beta_1)] \\ \quad +\sin\varphi_1 \cos(\varphi_2+\varphi_3)J_0(\beta_2)J_3(\beta_1) \\ \quad -\cos\varphi_1 \sin(\varphi_2+\varphi_3)J_1(\beta_2)J_0(\beta_1) \\ \quad -\cos(\varphi_2+\varphi_3) \sin(\varphi_2+\varphi_3)J_0(\beta_2)J_1(\beta_2) \end{cases} \tag{8}$$

As seen, the third-harmonic frequency term is generated. By adjusting the three bias voltages, the maximum amplitude of $3\omega_{m1}$ can be theoretically obtained. The $3\omega_{m1}$ frequency component mainly consists of two parts: one comes from the direct modulation generated from MZM1 and the other from the input triple-frequency oscillation signal in the OEO loop. In the case of a stable injection-locked state, the SSB phase noise of the locked oscillation signal can be described as [34]:

$$\begin{aligned} &\left\langle \left| S_{locked-output}(f) \right|^2 \right\rangle \\ &= \frac{\cos^2(3\varphi_0)}{\cos^2(3\varphi_0) + (\frac{f}{\Delta\omega_{\max}})^2} \left\langle \left| S_{input-\text{tripling}}(f) \right|^2 \right\rangle \\ &+ \frac{(\frac{f}{\Delta f})^2}{\cos^2(3\varphi_0) + (\frac{f}{\Delta\omega_{\max}})^2} \left\langle \left| S_{free-\text{running}}(f) \right|^2 \right\rangle \end{aligned} \tag{9}$$

where $\left\langle \left| S_{locked-output}(f) \right| \right\rangle$ represents an ensemble average of the SSB phase noise of the output triple-frequency signal for the injection-locked OEO. $\left\langle \left| S_{input-tripling}(f) \right| \right\rangle$ and $\left\langle \left| S_{free-running}(f) \right| \right\rangle$ are the input triple-frequency signal generated by MZM1 and the OEO oscillation signal without injection, respectively. φ_0 is the constant phase difference between injected and locked signals. f is the frequency offset. In addition, $\Delta\omega_m$ is the locking range of this OEO system, which can be described as follows:

$$3\omega_1 - \omega_{free-running} \le \Delta\omega_{\max} = \frac{\omega_1}{Q}\frac{V_{input-tripling}}{V_{bias\,2}} \tag{10}$$

in which $\omega_{free-running}$ denotes the free running oscillation frequency of the OEO loop and Q denotes the quality factor for the resonator. $V_{input-tripling}$ is the amplitude of the triple-frequency signal that is modulated from MZM1. Therefore, according to Equations (9) and (10), within a small frequency-offset range, the SSB phase noise of the triple-frequency signal is mainly determined by the input RF signal. Within higher frequency-offset ranges, it is mainly limited by the OEO loop. In our system, the high Q characteristic of the OEO is fully utilized to realize frequency multiplication independent of phase noise deterioration.

3. Results and Discussion

A schematic diagram of the proposed frequency-tripled signal generator system is shown in Figure 2. A distributed feedback laser diode (DFB-LD) outputs a CW with a wavelength of 1546.95 nm. The output power is 10.36 dBm. The CW is modulated by the DPMZM with a RF driving signal generated by a microwave frequency synthesizer (MFS, HEWLETT PACKARD E8257D). The frequency of the driving signal is f_{m}. A 2-km single-mode fiber (SMF) is placed after the DPMZM to act as the microwave energy-storage element of the OEO resonator. After the SMF, the light field is divided into two parts by an optical coupler: one part is monitored by an optical spectrum analyzer (Anritsu MS9710C, OSA), and the other part is converted into the electrical domain by a PD with a bandwidth of 22 GHz. A high-Q electrical bandpass filter (EBPF) is used to select the desired oscillation mode and suppress other modes to achieve single-mode operation. The center frequency of the EBPF ($f_{\mathrm{EBPF}} = 3f_{\mathrm{m}}$) is 20 GHz, and the 3-dB bandwidth is 100 MHz. After a power splitter (PS1), the microwave signal is split into two branches. One branch is applied to the DPMZM, and the other branch is further divided into an electrical spectrum analyzer (Agilent 8564EC) and a phase noise analyzer (RS FSWP50). When the optoelectronic feedback loop is closed and the open loop gain is greater than the loss, optoelectronic oscillation is established. By adjusting the biases of the DPMZM and the power of the input RF signal, the OEO works in the injection-locked state [35]. A microwave signal with a frequency of f_{EBPF} is generated. As the DPMZM is known to suffer from bias drift, in the following experiments, the laboratory temperature is stable at 25 °C. For polarization stability, polarization-maintaining fibers are used to connect parts of the optical path of the system, such as the output fiber pigtail of the DFB-LD and the input and output fiber pigtail of the DPMZM. For the environmental vibration, the whole system is placed on a vibration isolation platform.

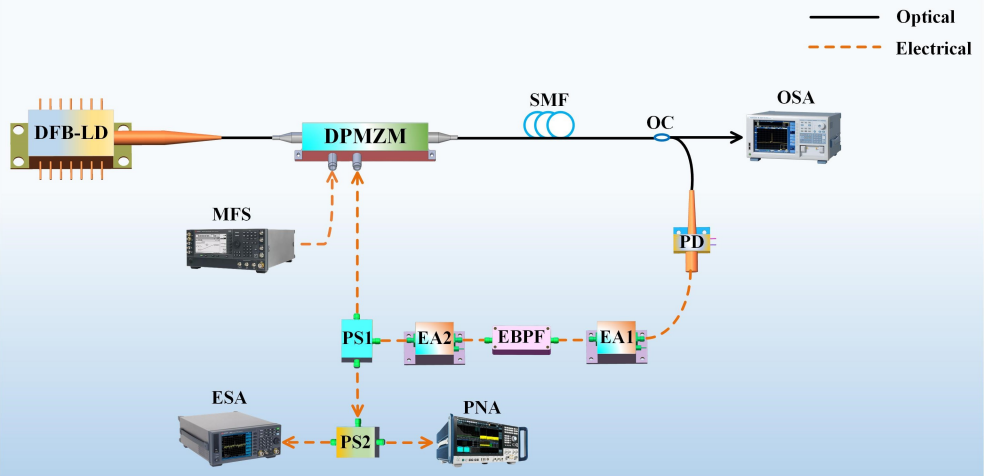

Figure 2. Experimental setup of the frequency-tripled signal generator system. DFB-LD: distributed feedback laser diode, DPMZM: dual-parallel Mach–Zehnder modulator, SMF: single-mode fiber, OC: optical coupler, PD: photodetector, EA: electrical amplifier, EBPF: electrical bandpass filter, PS: power splitter, MFS: microwave frequency synthesizer, ESA: electrical spectrum analyzer, PNA: phase noise analyzer, OSA: optical spectrum analyzer.

First, the DPMZM is described to illustrate the principle of the proposed system. The DPMZM has a 3-dB bandwidth of 30 GHz and a half-wave voltage of 3.5 V, which is only driven by a 6.673-GHz RF driving signal generated by the MFS. In other words, the OEO loop is disconnected and there is no EO feedback. The bias voltages V_{bias1}, V_{bias2}, and V_{bias3} for the DPMZM are adjusted to 3.7 V, 0.07 V, and 0.3 V, respectively. It is worth mentioning that the three biases are adjusted according to the experimental results. Specifically, when the power of the third-order harmonic in the electrical spectrum is at its maximum, we think that the bias values are more appropriate. In addition, although the V_{bias1} exceeds the

half-wave voltage, according to the modulation curve of the modulator, the effect on the RF amplitude in this case can be ignored. As shown in Figure 3, ±3-order sidebands are generated in the optical spectrum of the RF signal. The corresponding electrical spectrum after optical-to-electrical conversion is given in Figure 4. Here, the power ratios of the first harmonic to the second-order/third-order harmonics are 26.5 dB and 30.0 dB, respectively. It should be mentioned that, although the third-order sideband in the optical spectrum is slightly stronger than the second-order sideband, due to the PD bandwidth, the intensity of the 20.019 GHz component in the electrical spectrum is weaker than the 13.346 GHz component.

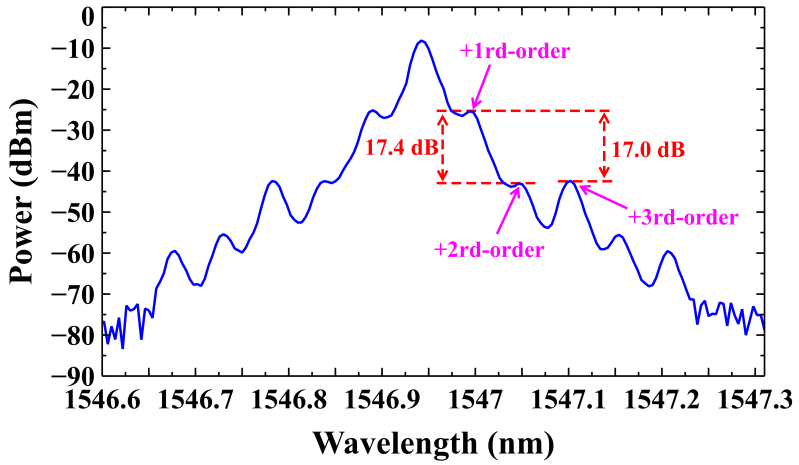

Figure 3. Measured optical spectrum of the DPMZM output.

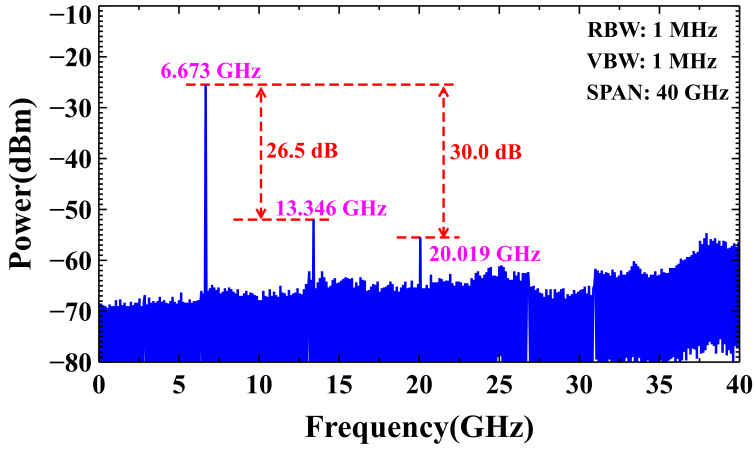

Figure 4. Measured electrical spectrum of the DPMZM output.

In order to describe the bias stability of the DPMZM, the power values of the third-order harmonics at 10-s intervals over a 10-min period are recorded. The black dots in the Figure 5 represent the power values corresponding to each time point. The power fluctuation range is approximately less than 1 dB, which mainly comes from the three bias fluctuations. However, this power fluctuation is still very small, and in subsequent experiments, the system can still output a high-quality triple-frequency signal.

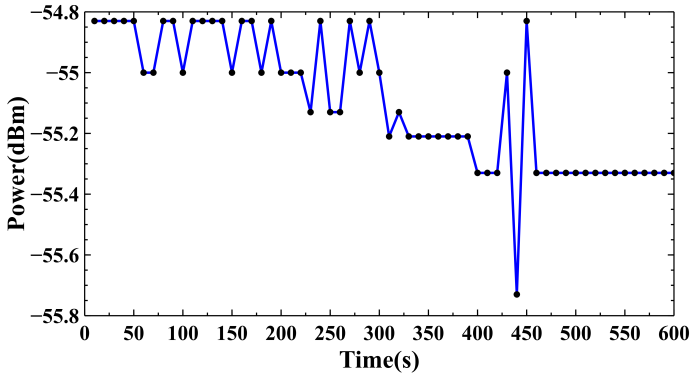

Figure 5. Long-term power drift of the third-order harmonics within 10-min measurement.

Second, the free-running OEO is operated based on Figure 2, in which the RF signal is disconnected. When the total gain of the cavity is greater than unity, the OEO starts self-oscillation from noise. The oscillation frequency is determined by the center frequency of the EBPF. Figure 6 shows the electrical spectrum of the generated 20.019 GHz microwave signal. Here, the stronger side modes present a frequency periodicity of 103.3 kHz, which corresponds to the free spectral range (FSR) of the 2-km OEO resonant cavity. In addition, the measured SMSR is 19.6 dB. Since the side modes are close to each other, mode hopping is observed in the experiment. It is well known that optical power is also an important parameter for OEO. Generally, when the optical power is too weak, the OEO cannot oscillate. However, when the optical power is too strong, the PD may be saturated or even damaged. Therefore, a DFB-LD with an output power of 10.36 dBm is used as a light source to ensure that the PD is not saturated.

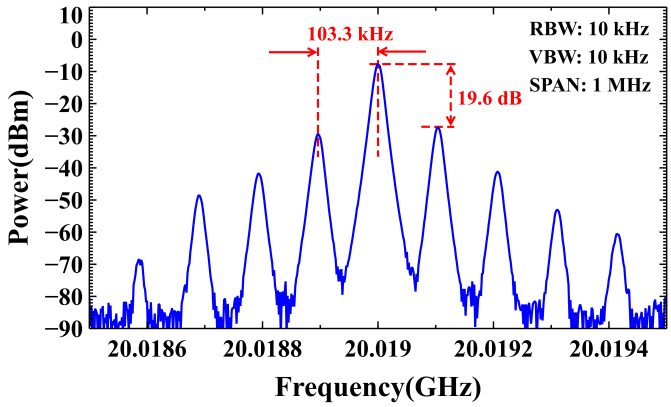

Figure 6. Measured electrical spectrum of the free-running OEO output.

Next, the RF signal (6.673 GHz) is applied to the DPMZM. Moreover, the 20.019 GHz microwave signal generated by the OEO is also used as a driving signal for the DPMZM. By controlling the power of the two driving signals and the bias voltages applied to the DPMZM, the OEO works under injection-locked conditions based on the RF signal. As shown in Figure 7a, a frequency-tripled microwave signal with a completely suppressed RF signal component is generated. A detailed view of the frequency-tripled microwave signal is given in Figure 7b. Due to the high Q value of the optical storage elements, a strong single-mode microwave signal with a frequency of 20.019 GHz is successfully obtained. The residual mode components are effectively suppressed by a ratio of 64.8 dB. Compared with Figure 6, the severe side modes can be significantly suppressed with the injection-locking scheme. Compared with the results of the other proposed schemes [18,19,30,31], a clear improvement in the performance in terms of an SMSR above 20 dB is achieved. Additionally, a magnified view of the electrical spectrum with a span of 100 Hz and a

resolution bandwidth (RBW) of 1 Hz is shown in Figure 7c. A high-purity frequency-tripled microwave signal is successfully obtained.

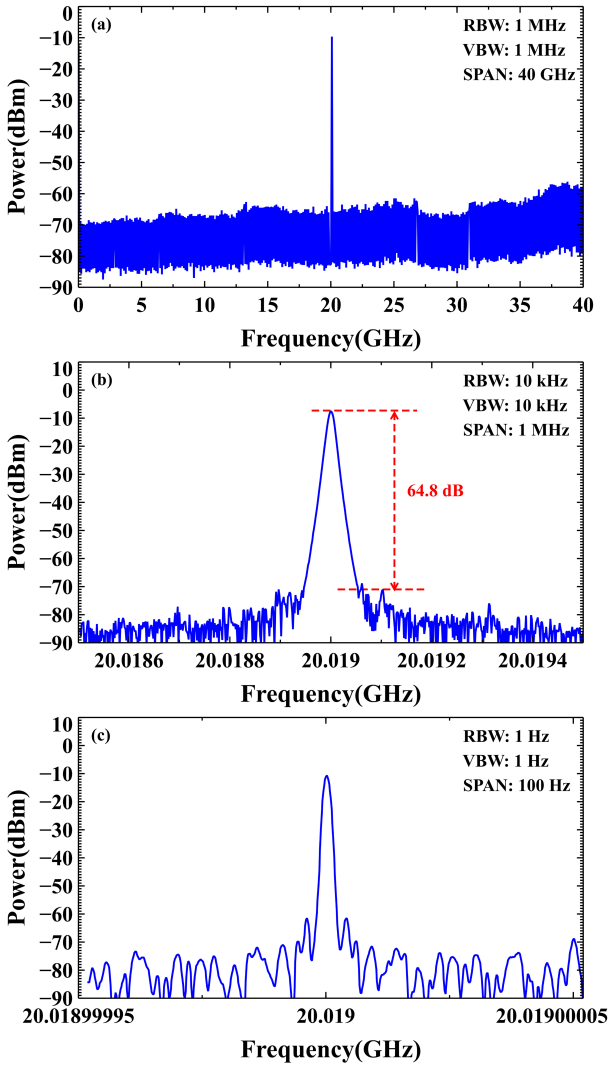

Figure 7. Measured RF spectra of the 20.019 GHz frequency-tripled microwave signal. (**a**) RBW = 1 MHz. VBW = 1 MHz. (**b**) RBW = 10 kHz. VBW = 10 kHz. (**c**) RBW = 1 Hz. VBW = 1 Hz.

To illustrate the stability of the proposed system, using the "Max Hold" function of the ESA, a long-term frequency stability test in a frequency window of 100 Hz is taken, which is shown in Figure 8. One can read that the frequency drift range is only 2 Hz within 10 min. It can be concluded that the frequency stability is relatively high.

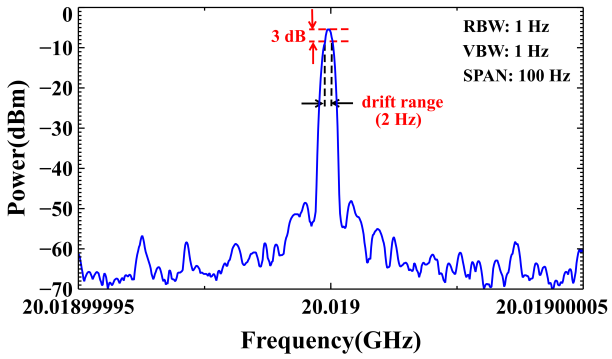

Figure 8. Long-term frequency drift within 10-min measurement with a span of 100 Hz.

To further evaluate the signal quality in detail, the SSB phase noise of the input RF signal, simulated frequency-tripled signal and injection-locked OEO signal are measured. The SSB curves under different operation conditions are shown in Figure 9. Here, the red dotted line is the input 6.673 GHz RF signal, and the phase noise value is read as −92 dBc/Hz@10 kHz. For the traditional electronic multiplier, the corresponding SSB phase noise always follows the deterioration rule shown in (11) [36]:

$$S_\varphi(f)_{out} = S_\varphi(f)_{in} + 20\log_{10}(N) \tag{11}$$

where $S_\varphi(f)_{out}$ and $S_\varphi(f)_{in}$ are the SSB phase noise values of the multiplier output and the input RF signal, respectively. N represents the frequency multiplication factor. As a result, if the input RF signal frequency is tripled, that is, $N = 3$, then the SSB phase noise of its triple-frequency signal deteriorates by 9.5 dB. We perform a simulation to evaluate the phase noise deterioration, denoted by the black dotted line in Figure 9. In contrast, the proposed photonic frequency multiplication yields the lowest phase noise, with a value of −126 dBc/Hz@10 kHz, which is shown in Figure 9 as the blue solid line. Compared with the input RF signal and the simulated electric triple frequency module, its value has significantly improved by 34 dB and 43.5 dB, respectively. Our system clearly makes full use of the advantages of the OEO long cavity and low phase noise, which avoids the phase noise deterioration in an electrical tripler. Although only one frequency is generated in this system, theoretically, as long as the device bandwidth is large enough, the system can generate a higher-frequency signal. Specifically, the tunability of the proposed system is mainly limited to the bandwidth of the DPMZM, PD, EA, and the center frequency of the EBPF. In the experiment, the 3-dB bandwidths of the DPMZM, PD, and EA are 30 GHz, 22 GHz, and 40 GHz, respectively. The center frequency of the EBPF is 20 GHz with a 3-dB bandwidth of 100 MHz. It's worth mentioning that the frequency of the triple-signal is equal to the center frequency of the EBPF. Therefore, considering our lack of tunable high-frequency EBPF, the experiment only demonstrates the injection of 6.673-GHz RF signal.

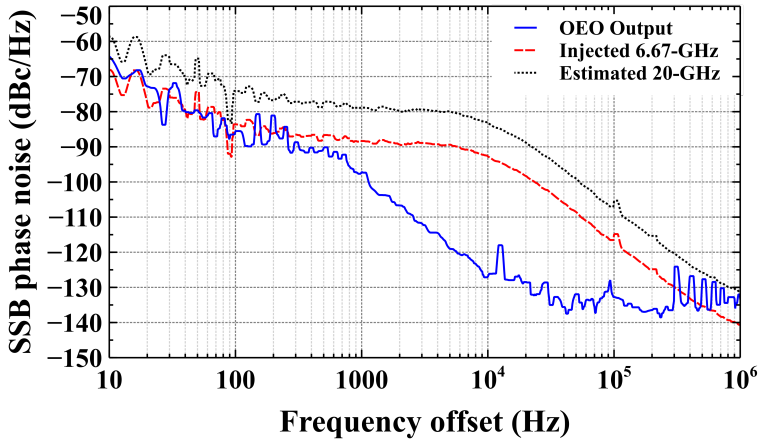

Figure 9. SSB phase noise of the injected 6.673 GHz RF signal (red dotted line), the estimated 20.019 GHz performance (black dotted line), and the measured 20.019 GHz frequency-tripled signal output from the OEO.

4. Conclusions

In summary, we have theoretically and experimentally demonstrated a novel approach to achieve a frequency-tripled signal based on an injection-locked OEO. In this system, the injected RF signal and the oscillation signal of the OEO are used as the driving signals of the DPMZM. When the oscillation signal of the OEO is locked by the externally injected RF signal, a triple-frequency signal with low SSB phase noise and a high SMSR is successfully generated by a photonic approach. Compared with the previously reported electrical

frequency multiplication systems, the proposed scheme has three advantages: (1) The injection-locked OEO can effectively suppress the RF signal and achieve a strong single-mode microwave signal with a high SMSR of 64.8 dB. (2) The SSB phase noise of the output is independent of electrical tripler phase noise deterioration. In the experiment, the SSB phase noise of the triple-frequency signal at 20.019 GHz is −126 dBc/Hz@10 kHz, which is 34 dB better than the input RF signal and optimized 43.5 dB than the simulated electrical frequency tripler. (3) The proposed approach combines the functions of low-phase-noise microwave generation and frequency up-conversion and may find various applications not only in radio-over-fiber systems but also in signal processing and photonic frequency mixing areas.

Author Contributions: Conceptualization, H.L. and S.J.; software, H.L., C.M., X.H., X.S. and Y.G.; validation, H.L.; writing—original draft preparation, H.L.; writing—review and editing, S.J., J.W. and J.Y.; supervision, S.J., J.W. and J.Y. All authors have read and agreed to the published version of the manuscript.

Funding: This research was supported by the National Natural Science Foundation of China under Grant 62005194.

Institutional Review Board Statement: Not applicable.

Informed Consent Statement: Not applicable.

Data Availability Statement: The raw data supporting the conclusions of this article will be made available by the authors on request.

Conflicts of Interest: The authors declare no conflicts of interest.

References

1. Ummethala, S.; Harter, T.; Koehnle, K.; Li, Z.; Muehlbrandt, S.; Kutuvantavida, Y.; Kemal, J.; Mar-in-Palomo, P.; Schaefer, J.; Tessmann, A.; et al. Thz-to-optical conversion in wireless communications using an ultra-broadband plasmonic modulator. *Nat. Photonics* **2019**, *13*, 519–524. [CrossRef]
2. Zhang, Z.; Liu, Y.; Stephens, T.; Eggleton, B.J. Photonic radar for contactless vital sign detection. *Nat. Photonics* **2023**, *17*, 791–797. [CrossRef]
3. Jin, J.; Geng, S.; Shu, L.; Jiang, P.; Shao, X.; Han, C.; Ren, L.; Li, Y.; Yang, L.; Wang, X. High-strength and crack-free welding of 2024 aluminium alloy via zr-core-al-shell wire. *Nat. Commun.* **2024**, *15*, 1748. [CrossRef] [PubMed]
4. Wang, C.-X.; Haider, F.; Gao, X.; You, X.-H.; Yang, Y.; Yuan, D.; Aggoune, H.M.; Haas, H.; Fletcher, S.; Hepsaydir, E. Cellular architecture and key technologies for 5g wireless communication networks. *IEEE Commun. Mag.* **2014**, *52*, 122–130. [CrossRef]
5. Chen, Y. Photonic generation and transmission of triangular and square waveforms with a large repetition rate tunable range. *J. Light. Technol.* **2018**, *36*, 3293–3301. [CrossRef]
6. Xue, C.; Ji, S.; Wang, A.; Jiang, N.; Qiu, K.; Hong, Y. Narrow-linewidth single-frequency photonic microwave generation in optically injected semiconductor lasers with filtered optical feedback. *Opt. Lett.* **2018**, *43*, 4184–4187. [CrossRef]
7. Hao, T.; Tang, J.; Domenech, D.; Li, W.; Zhu, N.; Capmany, J.; Li, M. Toward monolithic integration of oeos: From systems to chips. *J. Light. Technol.* **2018**, *36*, 4565–4582. [CrossRef]
8. Yao, J. Microwave photonics. *J. Light. Technol.* **2009**, *27*, 314–335. [CrossRef]
9. Ding, T.; Tang, Y.; Sun, X.; Huang, Y.; Jiang, B.; Liu, J.; Li, Z.; Zheng, Y.; Chen, X. Experimental demonstration of te/tm polarization-independent frequency upconversion assisted by polarization coupling. *Chin. Opt. Lett.* **2023**, *21*, 121901. [CrossRef]
10. Guo, Q.; Fan, S.; Yin, X.; Jiao, B.; Mu, J.; Ming, N.; Guo, L.; Yuan, J.; Wang, K.; Zhang, X. Highly sensitive frequency upconversion detection from 1 to 3 THz with oh1 crystal. *Opt. Express* **2023**, *31*, 38970–38976. [CrossRef]
11. Zaldívar-Huerta, I.E.; Mbuebue, B.T.; García-Juárez, A.; Kanyinda, E.-Y.T.; Rojas-Laguna, R.; Lee, M.W. An experimental alternative of microwave signal generation through an optical heterodyning technique using a multimode laser diode and a tunable dfb laser. *IEEE Lat. Am.* **2024**, *22*, 512–518. [CrossRef]
12. Liu, G.; Lu, Z.; Liu, J.; Poole, P.J.; Mao, Y.; Xie, X.; Vachon, M.; Song, C.-Y.; Barrios, P. Directly Modulated Quantum-Dash Mode-Locked Lasers for Millimeter-Wave over Fiber Applications. In *Terahertz, RF, Millimeter, and Submillimeter-Wave Technology and Applications XVII*; SPIE: Bellingham, WA, USA, 2024; Volume 12885, pp. 137–140.
13. Yuan, J.; Zhang, M.; Mei, Y.; Liu, Q.; Liu, J. Photonic generation of millimeter-wave and multi-waveform signals based on external modulation and polarization control. *Appl. Opt.* **2022**, *61*, 8967–8973. [CrossRef]
14. Dar, A.B.; Ahmad, F.; Jha, R.K. Filterless optical millimeter-wave generation using cascaded-parallel mach–zehnder modulators with tunable frequency multiplication factor. *Opt. Quantum Electron.* **2021**, *53*, 1–15. [CrossRef]

15. Wu, Z.; Cao, C.; Zeng, X.; Feng, Z.; Shen, J.; Yan, X.; Wang, B.; Su, X. Filterless radio-over-fibersystem to generate 40 and 80 ghz millimeter-wave. *IEEE Photonics J.* **2020**, *12*, 1–13.
16. Du, C.; Zhou, W.; Wang, Y.; Wang, M.; Wang, D.; Wang, K.; Dong, W.; Zhang, X. Photonic millimeter-wave ultrawideband signal generation using frequency upconversion based on the stimulated brillouin scattering effect. *Opt. Lett.* **2018**, *43*, 4915–4918. [CrossRef]
17. Zhang, Z.; Xu, Y.; Luo, X.; Chen, M.; Bao, H. Passively stabilized brillouin fiber laser frequency combs for ultralow-noise microwave generation. *Appl. Phys. Lett.* **2024**, *124*, 211105. [CrossRef]
18. Li, X.; Jeon, C.; Pan, S.; Kim, J. Low-noise repetition-rate multiplication by injection locking and gain-saturated amplification. *IEEE Photonics Technol. Lett.* **2019**, *31*, 997–1000. [CrossRef]
19. Jeon, C.J.; Zhang, S.; Shin, J.; Kim, J. Highly tunable repetition-rate multiplication of mode-locked lasers using all-fibre harmonic injection locking. *Sci. Rep.* **2018**, *8*, 13875. [CrossRef]
20. Chen, Y.; Wen, A.; Shang, L. Analysis of an optical mm-wave generation scheme with frequency octupling using two cascaded mach–zehnder modulators. *Opt. Commun.* **2010**, *283*, 4933–4941. [CrossRef]
21. Huang, Z.; Cao, C.; Feng, Z.; Zeng, X.; Wu, J.; Wu, Q.; Wu, Z. Filterless radio-over-fiber system that generates 80 and 160 ghz millimeter waves based on two mzms. *Appl. Opt.* **2021**, *60*, 4871–4877. [CrossRef] [PubMed]
22. Zhou, H.; Fei, C.; Zeng, Y.; Tan, Y.; Chen, M. A rof system based on 18-tuple frequency millimeter wave generation using external modulator and soa. *Opt. Fiber Technol.* **2021**, *61*, 102402. [CrossRef]
23. Awsaj, M.K.; Al-Mashhadani, T.F.; Al-Mashhadani, M.K.S.; Ali, A.Y.; Zan, M.S.D.; Arsad, N. Multiwavelength fiber laser sources with 60 GHz brillouin frequency shift. *Opt. Quantum Electron.* **2023**, *55*, 528. [CrossRef]
24. Xu, L.; Bai, G.-F.; Tang, J.; Tang, Y.-L.; Jiang, Y. All-optical microwave oscillator using cross-gain modulation of semiconductor optical amplifier and cascaded stimulated brillouin scattering effects in optical fiber. *Opt. Commun.* **2022**, *514*, 128167. [CrossRef]
25. Chen, M.; Xu, Y.; Zhang, Z.; Luo, X.; Bao, H. Stabilized brillouin laser with sub-hz fundamental linewidth aided by frequency shifted optical injection locking. *APL Photonics* **2024**, *9*, 026103. [CrossRef]
26. Li, L.; Chen, J.; Zhang, J.; Yao, J. Stepped-frequency microwave waveform generation based on a fourier domain mode-locked optoelectronic oscillator. *IEEE Photonics Technol. Lett.* **2024**, *36*, 305–308. [CrossRef]
27. Ma, Y.; Linghu, S.; Chen, B.; Gu, F. Continuous ultra-wideband signal regeneration in random optoelectronic oscillators through injection locking. *Opt. Express* **2024**, *32*, 9847–9856. [CrossRef]
28. Liu, A.; Dai, J.; Xu, K. Stable and low-spurs optoelectronic oscillators: A review. *Appl. Sci.* **2018**, *8*, 2623. [CrossRef]
29. Fu, J.; Dai, Z.; Han, X.; Yao, J. Wavelength-space parity-time symmetric optoelectronic oscillator using a chirped fiber bragg grating. *IEEE Photonics Technol. Lett.* **2023**, *36*, 187–190. [CrossRef]
30. Li, C.; Mao, J.; Dai, R.; Zhou, X.; Jiang, J. Frequency-sextupling optoelectronic oscillator using a mach–zehnder interferometer and an fbg. *IEEE Photonics Technol. Lett.* **2016**, *28*, 1356–1359. [CrossRef]
31. Wang, H.; Wu, B.; Zhou, H.; Wang, W.; Xu, G. Optical tunable frequency-doubling oeo using a chirped fbg based on orthogonally polarized double sideband modulation. *Photonics* **2023**, *10*, 1002. [CrossRef]
32. Rani, A.; Kedia, D. Mathematical analysis of 24-tupled mm-wave generation using cascaded mzms with polarization multiplexing for rof transmission. *Opt. Quantum Electron.* **2024**, *56*, 193. [CrossRef]
33. Jiang, Y.; Ma, C.; Bai, G.; Qi, X.; Tang, Y.; Jia, Z.; Zi, Y.; Huang, F.; Wu, T. Photonic microwave waveforms generation based on time-domain processing. *Opt. Express* **2015**, *23*, 19442–19452. [CrossRef]
34. Lee, K.-H.; Kim, J.-Y.; Choi, W.-Y. Injection-locked hybrid optoelectronic oscillators for single-mode oscillation. *IEEE Photonics Technol. Lett.* **2008**, *20*, 1645–1647. [CrossRef]
35. Fan, Z.; Su, J.; Lin, Y.; Jiang, D.; Chen, Y.; Li, X.; Qiu, Q. Injection locking and pulling phenomena in an optoelectronic oscillator. *Opt. Express* **2021**, *29*, 4681–4699. [CrossRef]
36. Liu, B.; Diao, S.; Lin, F. An injection-locked frequency doubler with improved odd-order spur suppression. In Proceedings of the 2014 IEEE International Wireless Symposium (IWS 2014), Xi'an, China, 24–26 March 2014; IEEE: Piscataway Township, NJ, USA, 2014; pp. 1–4.